ACS Catalysis

Research Article

pubs.acs.org/acscatalysis

Morphology and Active-Site Engineering for Stable Round-Trip Efficiency Li–O_2 Batteries: A Search for the Most Active Catalytic Site in Co_3O_4

Kyeongse Song,[†] Eunbi Cho,[†] and Yong-Mook Kang*[,†]

[†]Department of Energy and Materials Engineering, Dongguk University-Seoul, Seoul 100-715, Korea

Supporting Information

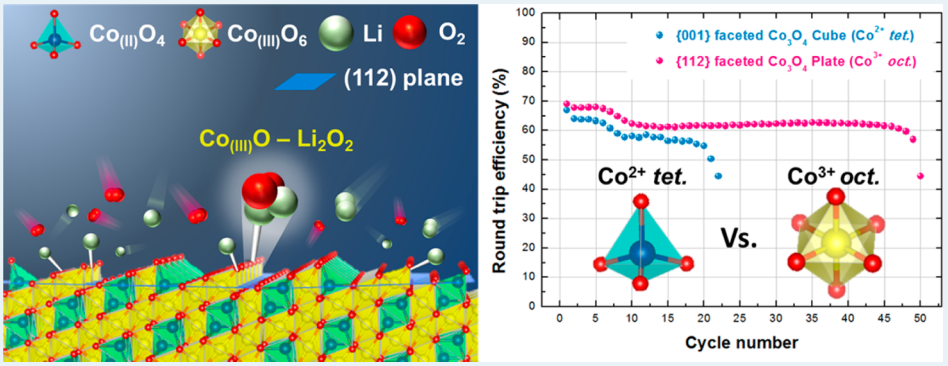

ABSTRACT: For the purpose of finding the catalytic active site for the oxygen reduction reaction (ORR) and the oxygen evolution reaction (OER) in the crystal structure of Co_3O_4, a {100} faceted Co_3O_4 cube enclosed by only a Co^{2+} site and a {112} faceted Co_3O_4 plate also exposing a Co^{3+} site was adopted as a catalyst for lithium–oxygen (Li–O_2) batteries. Thus, we found that the Co^{3+} site plays the crucial role of determining the adsorption properties of reactants, enabling high round-trip efficiency and cyclic stability, as well as the morphology of discharge products such as Li_2O_2.

KEYWORDS: *lithium–oxygen batteries, catalysts, cobalt oxides, electrochemistry, lithium peroxides*

Transition metal oxides have been widely employed in various fields because of their intrinsic magnetic, mechanical, optical, and electrical properties.[1−5] For designing tailored materials that can be applied to next-generation devices, the above-mentioned properties have been properly tuned by controlling their structure and size over the past few decades.[6−13] Among the various transition metal oxides, cobalt oxides—in which the Co^{2+} and Co^{3+} ions occupy the tetrahedral and octahedral sites, respectively—have proven valuable as solid-state sensors[14] electrochemical energy storage materials,[15−17] magnetic materials,[18,19] and catalysts.[20] Specifically, Co_3O_4 catalysts have been used for the oxidation of carbon monoxide (CO),[21−24] the decomposition of nitrous oxides (N_2O),[25,26] methanol (CH_3OH) combustion,[27] methane (CH_4) combustion,[28] toluene (C_7H_8) combustion,[29] and so on.[30−33] In order to maximize the catalytic activity, nanostructured Co_3O_4 materials have been designed and investigated extensively. Enlarging the surface area of catalysts,[34−36] controlling the exposed catalytic active site,[37−39] and surface charge engineering[40,41] can successfully enhance catalytic activity. In particular, determining the most advantageous exposed facet of the Co_3O_4 nanostructure derived from its morphology could lead to a breakthrough in its catalytic activity owing to the density change of the active site on the surface that enables proper bond strength with the reactant, resultantly promoting catalytic activity.[9−23,30−33] It is well-known that chemisorption and bond strength between the catalytic active site and reactant determine their catalytic efficiency based on Sabatier's principles as well as the d-band orbital center model.[42,43] For CO oxidation and CH_4 combustion, the {110} and {112} facets of Co_3O_4 nanocrystals have higher catalytic activities than the {100} and {111} facets because of the more abundant catalytically active Co^{3+} sites on the former.[21−23,30−33] This kind of validation of the active sites of catalyst materials has accelerated the efficient design of highly active catalysts. Therefore, the search for the most active catalytic sites should begin with a suggestion of the most appropriate catalyst material.[21−23,30−33]

Recently, the utilization of catalysts has been extended to lithium–oxygen (Li–O_2) batteries, which have emerged as a promising technology for electric vehicles (EVs) and energy storage systems (ESSs) due to their high theoretical energy density (11 140 $Wh{\cdot}kg^{-1}_{(Li)}$) comparable to gasoline engines (13 000 $Wh{\cdot}kg^{-1}$). However, current Li–O_2 batteries have many limitations preventing their practical use, such as low round-trip efficiency and sluggish kinetics, which are associated

Received: June 9, 2015
Revised: July 22, 2015
Published: July 24, 2015

© 2015 American Chemical Society

DOI: 10.1021/acscatal.5b01196
ACS Catal. 2015, 5, 5116−5122

with the high thermodynamic stability of discharge products.[44−49] To alleviate these issues, various electrocatalyst design methods using noble metal nanoparticles, nanostructured transition metal oxides, and metal oxyhydroxides have been suggested to improve oxygen reduction reactions (ORR, during discharge) or oxygen evolution reactions (OER, during charging).[50−53] However, the active site of the catalyst materials governing the whole reaction is still not completely understood.[50−53]

Bruce's group examined the catalytic activity of various materials, such as Pt, $La_{0.8}Sr_{0.2}MnO_3$, Fe_2O_3, NiO, Fe_3O_4, Co_3O_4, CuO, and $CoFe_2O_4$.[54] In particular, Co_3O_4 with Co^{2+} as well as Co^{3+} induced a significantly reduced OER overpotential, whereas the performance of Li−O_2 cells including $CoFe_2O_4$ where Co^{2+} and Fe^{3+} ions occupy tetrahedral and octahedral sites revealed a relatively higher overpotential during OER, similar to that of Fe_2O_3. Therefore, we can presume that the reduced OER overpotential in Co_3O_4 was mainly due to the Co^{3+} ion and its $Co^{3+}O_6$ octahedral sites.

Based on the insight gained from these studies, we investigated the detailed correlation between catalytic activity and active site arrangement on the surface of catalyst materials for Li−O_2 batteries. Herein, a comparison between cube- and plate-shaped Co_3O_4 seems to be appropriate to demonstrate the significance of the exposed structure and related active-site arrangement in oxide-based catalysts for Li−O_2 batteries. From the previous observations, cube-shaped Co_3O_4 exposes six {001} planes, while plate-shaped Co_3O_4 is generally enclosed by two dominant {111} or {112} planes. Because the above-mentioned planes have different Co^{3+} concentrations, following the order of {112} > {110} ≫ {001}, it was possible to determine the active catalytic sites of Co_3O_4 by controlling its shape and surface facet.[21−23,30−33] Finally, we successfully demonstrated that the catalytic activity of Co_3O_4 is closely related to Li_2O_2 nucleation and that its dissociation is strongly correlated with the surface Co^{3+} sites, which was crucial to enhance Li−O_2 battery performance with oxide catalysts.

RESULTS AND DISCUSSION

To validate the active-site effect, different shape-controlled Co_3O_4 materials corresponding to the {001} terminated cube

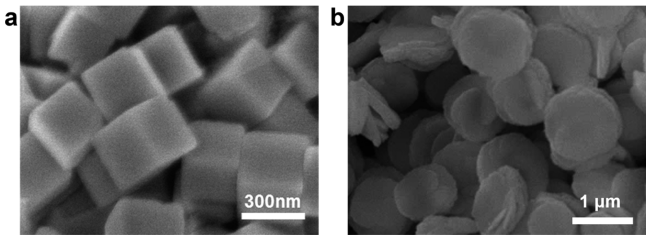

Figure 1. (a) SEM image of Co_3O_4 cube. (b) SEM image of Co_3O_4 plate.

and dominantly {112} enclosed plate were synthesized via the hydro- and solvothermal routes (see Experimental Section in Supporting Information). The crystal structure and morphology of Co_3O_4 materials were characterized by scanning electron microscopy (SEM), X-ray diffraction (XRD), and transmission electron microscopy (TEM). The SEM images indicate that the Co_3O_4 materials were well constructed into the cube shape with an average edge length of 300 nm and the plate shape with an average diameter of 1 μm (Figure 1 and Figure S1). The XRD

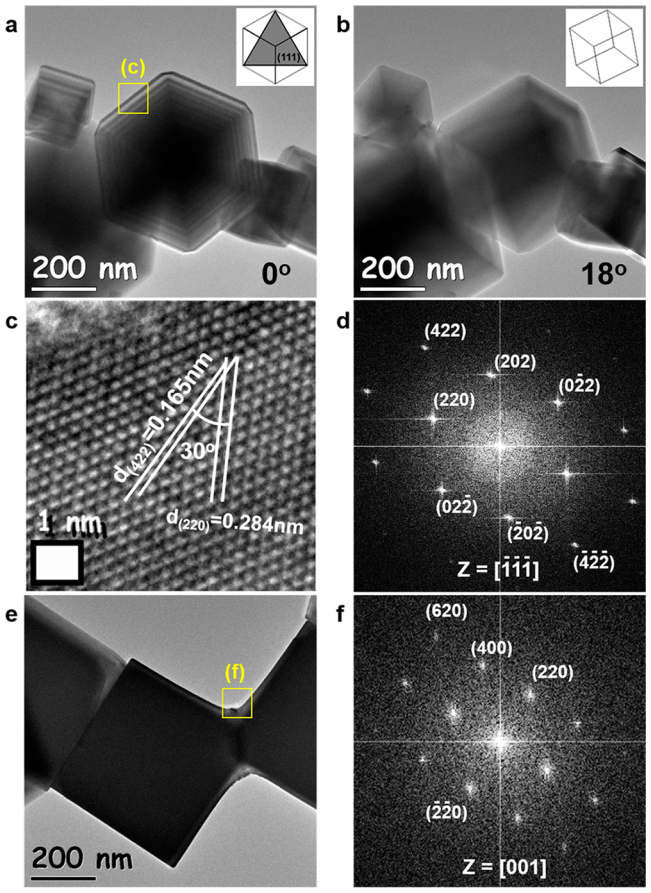

Figure 2. (a) TEM image of [111]-projected Co_3O_4 cube, its (b) 18° tilted TEM image, (c) HRTEM image, and (d) corresponding FFT pattern. (e) TEM image of [001]-projected Co_3O_4 cube and (f) corresponding FFT pattern.

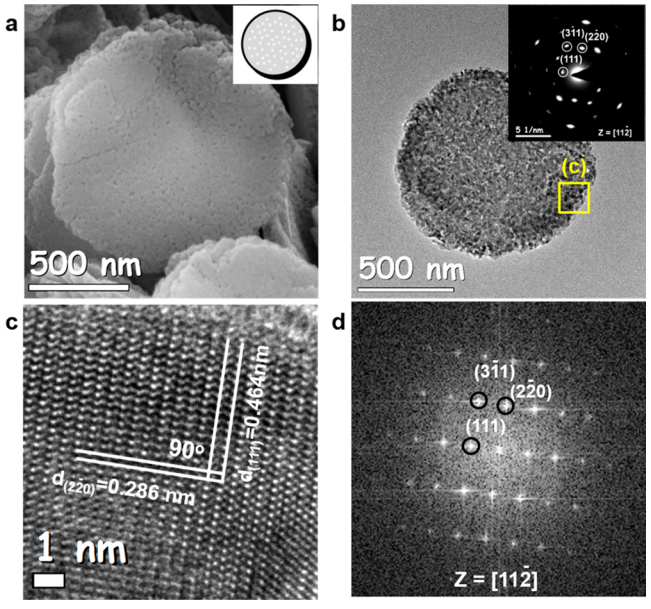

Figure 3. (a) SEM image, (b) TEM image (inset: SAED pattern), (c) HRTEM image, and (d) FFT pattern of Co_3O_4 plate.

patterns of the Co_3O_4 crystals clearly detected the typical diffraction peaks of spinel Co_3O_4 phases without exception (JCPDS no. 43-1003, space group: Fd/3m) (Figure S2). TEM

DOI: 10.1021/acscatal.5b01196
ACS Catal. 2015, 5, 5116−5122

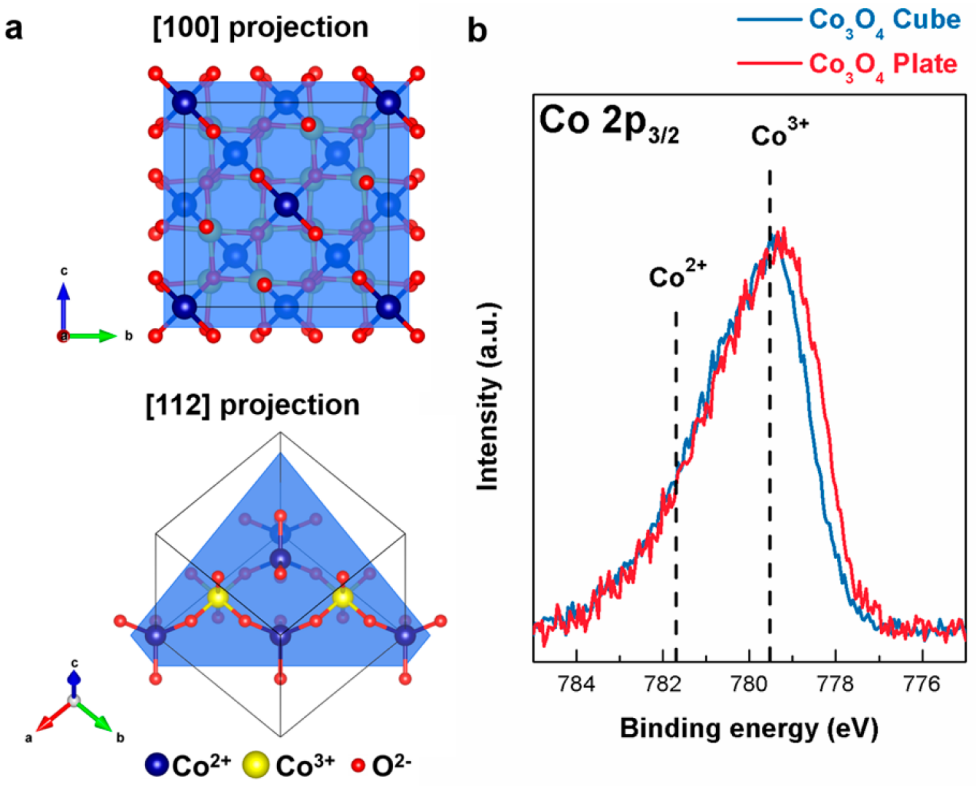

Figure 4. (a) Surface atomic configurations in (100) plane and (112) plane of Co_3O_4 crystal. The structure was drawn by VESTA software.[63] (b) Co $2p_{2/3}$ partial spectra of Co_3O_4 cube and Co_3O_4 plate.

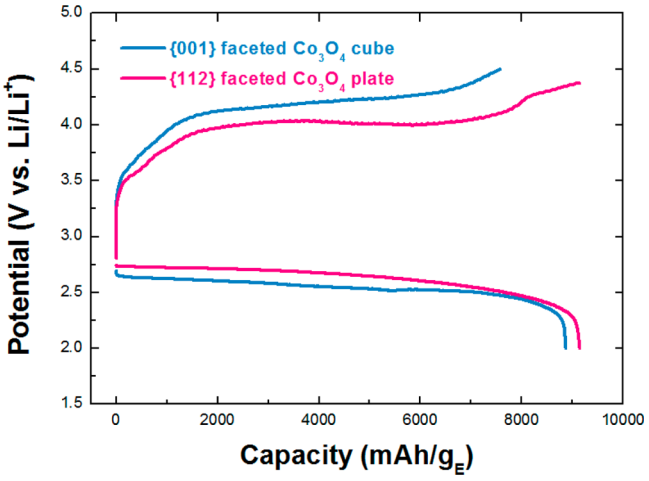

Figure 5. Initial galvanostatic discharge/charge potential profiles of {001} faceted Co_3O_4 cube and {112} faceted Co_3O_4 plate.

observation, as shown in Figure 2, unequivocally proved that our cube-shaped Co_3O_4 crystals were typically enclosed by six {001} planes. The hexagonal-shaped TEM image corresponding to the [111] projection of cube-shaped Co_3O_4 crystals is displayed in Figure 2a. The 18° tilted image obtained from Figure 2a shows that all presented Co_3O_4 crystals had cube-shaped morphologies (Figure 2b). Moreover, the enlarged high-resolution TEM (HRTEM) images obtained from the marked region in Figure 2a and its corresponding fast Fourier transform (FFT) image supported the [111] projected cube-shaped Co_3O_4 crystal models by confirming their lattice fringe and the interplanar angles between $d_{(422)}$ and $d_{(220)}$ as well as the [111] zone axis in the FFT pattern (Figures 2c and 2d). Finally, we confirmed the [001] projected Co_3O_4 crystal image and corresponding FFT pattern with the [001] zone axis, although the 500 nm-thick cube disrupted electron transmission in the core region. Thus, the resulting dominant exposed planes of Co_3O_4 cubes were all {001} facets (Figures 2e and 2f).

The crystalline microstructure of the plate-shaped Co_3O_4 can be seen in the FESEM and HRTEM images shown in Figure 3a and 3b. These images indicates that our Co_3O_4 plates became porous after the phase transition of $Co(OH)_2$ to Co_3O_4 by calcination. The selected area electron diffraction (SAED) pattern, as shown in the Figure 3b, proved that the single crystal nature with the [11-2] zone axis was well maintained, although there was some lattice mismatch. The surface HRTEM image obtained from the indicated solid region in Figure 3c obviously shows that the d spacings corresponding to the {220} and {111} planes are 0.286 and 0.464 nm, respectively. The 90° interplanar angle between the two specific planes proved that the {220} lattice fringe was (2−20) (Figure 3d). Analysis of the correlation of this atomic arrangement and its corresponding FFT pattern clearly demonstrated that our Co_3O_4 plates consisted of two (11-2) faceted basal planes and {100}, {110} enclosed side planes.

In order to distinguish the two kinds of surface facet planes in terms of the surface geometry and exposed site, the crystal structure model of Co_3O_4 was illustrated in Figure 4a, which was drawn by VESTA software.[63] The (100) plane of the Co_3O_4 surface was enclosed by only five Co^{2+} sites in a unit cell, whereas the (112) plane consisted of not only four Co^{2+} sites but also two Co^{3+} sites. Furthermore, the exposed surface oxidation states of Co_3O_4 crystals were confirmed by X-ray

DOI: 10.1021/acscatal.5b01196
ACS Catal. 2015, 5, 5116−5122

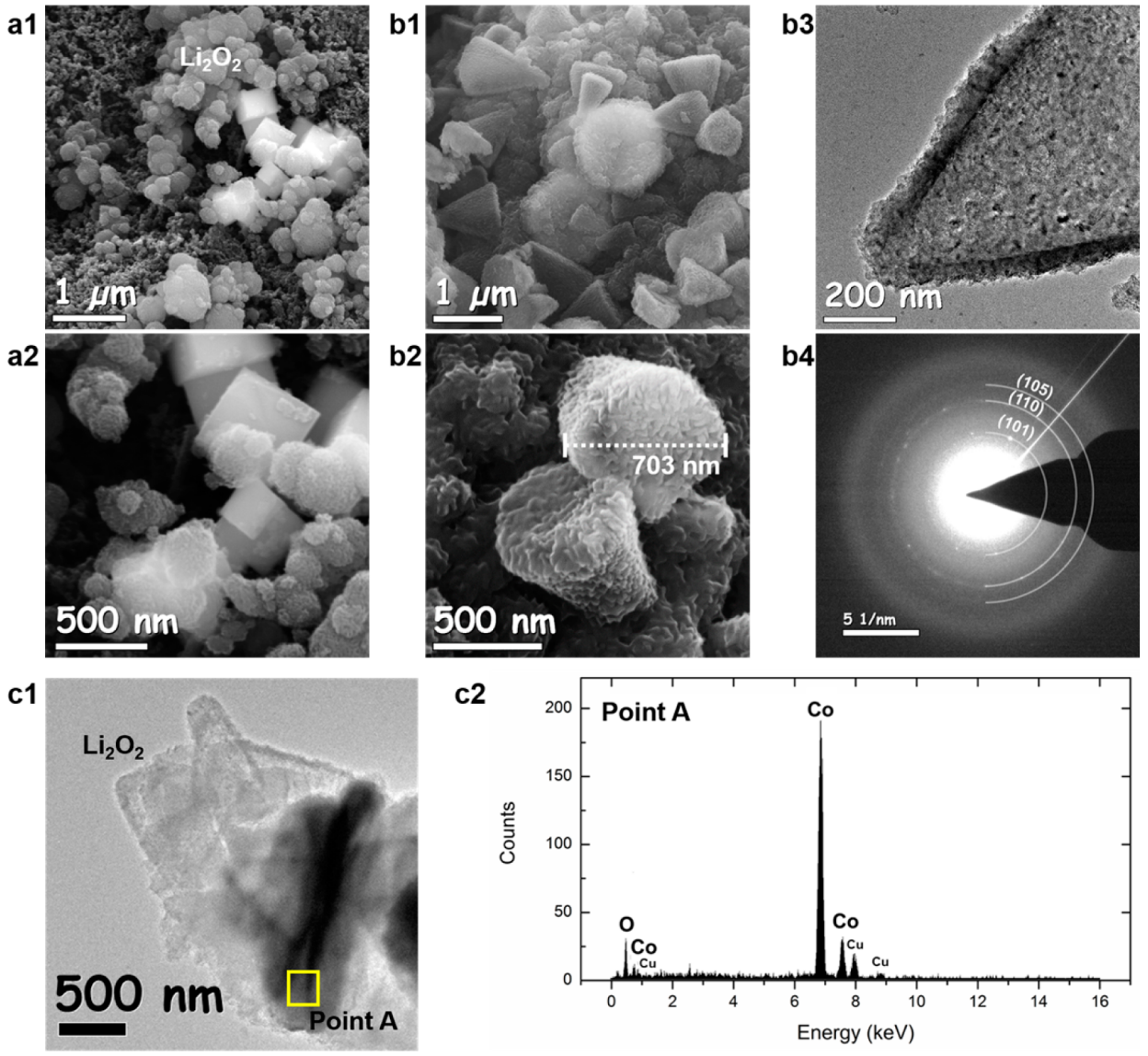

Figure 6. (a1, 2) SEM image of discharged electrode of {001} faceted Co_3O_4 cube. (b1, 2) SEM image of discharged electrode of {112} faceted Co_3O_4 plate. (b3) TEM image of angular cone-shaped Li_2O_2 and (b4) its corresponding SAED pattern. (c1) TEM image of {112} faceted Co_3O_4 plate with deposited Li_2O_2 (c2) EDS spectra of {112} faceted Co_3O_4 plate with deposited Li_2O_2, Cu signal comes from Cu grid.

photoelectron spectroscopy (XPS) even though the signals were not only obtained from the extreme outer surfaces. The Co $2p_{3/2}$ binding energy of the (112) faceted Co_3O_4 plate was negatively shifted, indicating that the exposed Co ions were more oxidized to Co^{3+} compared to the {001} faceted Co_3O_4 cube (Figure 4b). Some theoretical and experimental studies have indicated that charge control in exposed surface active-site and/or the control of their geometry can induce a couple of remarkable changes in catalyst properties.[21−23,30−33] This is because catalytic activities highly depend on the antibonding state and orbital occupation of catalyst, resulting in volcano-shaped dependence based on the influence of the adsorption, activation, and desorption features of the reactant on the catalyst surface during ORR and OER.[42,43] In this regard, we can expect that the catalytic activity of the {112} faceted Co_3O_4 plate would be very different from that of the {001} faceted Co_3O_4 cube due to the Co^{3+} site presence on the surface. Based on the above-mentioned work reported by Bruce's group, Li−O_2 cells, including the {112} faceted Co_3O_4 plate catalyst, may have higher round-trip efficiency.[54]

In order to identify the actual catalytic activity of Co_3O_4 crystals, porous cathodes including Co_3O_4 crystals as the catalysts were incorporated into a Swagelok-type cell. Co_3O_4 crystals were mixed with Ketjen black and binder (poly(vinylidene fluoride-hexafluoropropylene); PVdF-HFP copolymer) at a weight ratio of 75:15:10, respectively, in a solvent (*N*-methyl-2-pyrrolidone). Although the catalysts were included in a 1:1 ratio with carbonaceous materials by weight ratio generally, we had to use about twice the amount of catalyst to maximize the catalyst effect, even though it limited conductivity due to the semiconducting character of Co_3O_4 crystals. The slurry was uniformly pasted on carbon paper (gas diffusion layer; GDL) with the loading density of about 0.35 mg/cm^2. The prepared porous cathodes were dried at 120 °C in a vacuum oven. The cell used Li metal foil as the anode, 1 M $LiCF_3SO_3$ dissolved in tetra-ethylene glycol dimethyl ether (TEGDME) as the electrolyte, and glass fiber as the separator.

DOI: 10.1021/acscatal.5b01196
ACS Catal. 2015, 5, 5116−5122

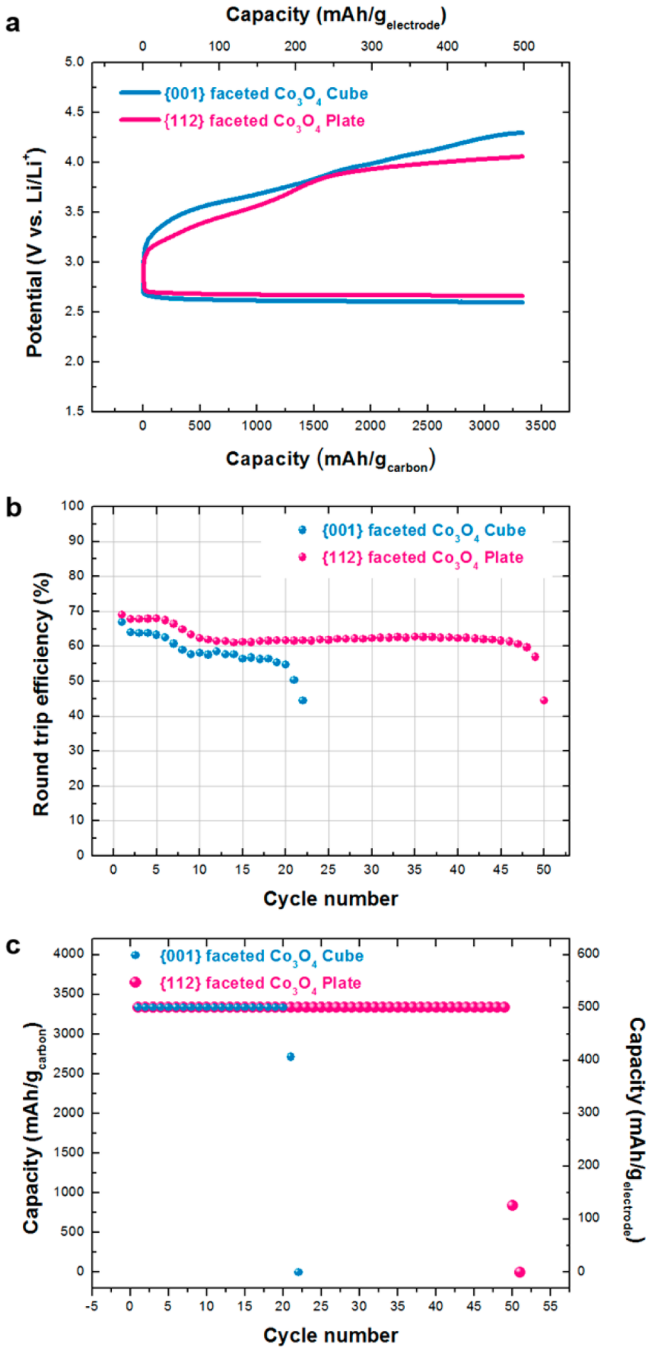

Figure 7. Electrochemical performance of Li−O_2 cells using {001} faceted Co_3O_4 cube and {112} faceted Co_3O_4 plate as cathode catalyst. (a) Initial galvanostatic discharge/charge profiles, (b) cyclic behaviors of each round-trip efficiency, and (c) discharge cycle capacity.

The cell assembly was carried out in an Ar-filled glovebox with less than 0.1 ppm each of oxygen and moisture. The cells were purged with O_2 gas (purity, 99.995%) for 10 min and closed after the pressure reached 1.1 atm. The electrochemical performance was then measured over the potential range of 2.0−4.5 V versus Li/Li^+ at a current density of 100 mA·$g_{(electrode)}^{-1}$ in galvanostatic mode. The initial potential profiles of the {112} faceted Co_3O_4 plate exhibited a relatively high capacity (9144 mAh/g) and low OER overpotential, enabling 67% round-trip efficiency to be attained, whereas the capacity and round-trip efficiency of the {001} faceted Co_3O_4 cube were each 8864 mAh/g and 60% as shown in Figure 5.

The morphological structure and composition of discharge products such as Li_2O_2 and Li_2O have been reported to be very important in determining the round-trip efficiency of Li−O_2 batteries.[55−60] Thus, the discharge products on the porous cathode including the {001} faceted Co_3O_4 cube and the {112} faceted Co_3O_4 plate were examined by SEM and TEM analyses. After the discharge process, the SEM images in Figures 6a1 and 6a2 indicated that the discharge product preferred growing on the Ketjen black than the Co^{2+}-site-terminated Co_3O_4 cube catalyst. The product was minimally attached also on part of the Co_3O_4 cube, which may be attributed the relatively high surface energy of the edge. On the other hand, the surface of the Co_3O_4 plate was perfectly encapsulated by the discharge product, having an unprecedented angular cone shape (Figure 6b1). The SEM image in Figure 6b2 indicated that the single angular cone-shaped discharge product consisted of small rod-like parts. To investigate the crystal structure and composition, the discharge products were analyzed by TEM, as shown in Figure 6b3 and 6b4. The SAED ring pattern obtained from the region of the individual angular cone-shaped discharge product was identical to those of the hexagonal Li_2O_2 phase. Moreover, the energy dispersive spectroscopy (EDS) data and TEM image in Figure 6c proved that the angular cone-shaped Li_2O_2 was better attached onto the (112) plane of Co_3O_4 than the sidewall. Thus, we can conclude that the nucleation sites like Co^{3+} and high surface energy atomic steps are meaningful features when materials were adopted as catalyst for Li−O_2 batteries. In order to find clear evidence for those of phenomenon, we also prepared a {111} faceted Co_3O_4 octahedron, which has a lower Co^{3+} concentration, albeit greater than the plate and cube, respectively, with the smallest BET surface area among the three samples. As a result, the catalytic activities are deeply attributed to the Co^{3+} concentration than surface area (Figure S3).

In this regard, we experimentally proved for the first time that the surface configuration of a catalyst can significantly control the morphology of Li_2O_2 like epitaxial growth in the vapor−liquid-solution interface. In addition, it is worthy of noting that the phenomenon was mainly due to the Co^{3+} site presence on the (112) plane. Therefore, we speculate that the Li adatom may initially bind to the oxygen of $Co^{3+}O_6$, yielding a $Co^{2+}O_6$−Li^+ bond, which is quite similar to the Co^{m+}/Co^0 redox couple reaction of the Co_3O_4 anode for lithium ion batteries. To improve the redox reaction rate in Li ion batteries, the morphological control dominating the surface atomic configuration has also been conducted, and it thus brought high capacity and rate capability.[61,62] On the basis of the correlation between this viewpoint and the reduction potential, we can easily understand why the discharge products preferred growing on the Co^{3+} site and did not bind with the Co^{2+} site ($Co^{2+}_{(aq)}$ + $2e^- \rightarrow Co_{(s)}$: $E^0(V) = -0.28$, $Co^{3+}_{(aq)} + e^- \rightarrow Co^{2+}_{(aq)}$: $E^0(V) = 1.81$).

For the stabilization of cycling, Li−O_2 batteries including Co_3O_4 catalysts were tested using a constant current−constant voltage (CC−CV) mode with potentiostatic steps at 4.5 V versus Li/Li^+ under limited capacity conditions (500 mAh·g^{-1}). This test protocol mainly assisted in limiting the formation of thermodynamically stable and insulating discharge products leading to irreversible capacity loss. Figure 7a exhibits the discharge and charge profiles of the Li−O_2 cells including the {001} faceted Co_3O_4 cube and the {112} faceted Co_3O_4 plate. The {112} faceted Co_3O_4 plate had a slightly low initial ORR and OER overpotential compared to the {001} faceted Co_3O_4

DOI: 10.1021/acscatal.5b01196
ACS Catal. 2015, 5, 5116−5122

cube electrode. Specifically, the initial cycle round-trip efficiency of the {112} faceted Co_3O_4 plate and {001} faceted Co_3O_4 cube attained 68.6% and 66.9%, respectively (Figure 7a). Similarly, the discharge products grew well on the {112} faceted Co_3O_4 plate with the lamellar shape, which provided a large surface-to-volume ratio enhancing electron transfer, while the surface of the {001} faceted Co_3O_4 cube maintained a clean and smooth surface (Figure S5). In Figure 7b, the Li−O_2 cell with the {001} faceted Co_3O_4 cube underwent very early round-trip efficiency decay during cycling, whereas the Li−O_2 cell with the {112} faceted Co_3O_4 plate clearly showed a more stable reaction thanks to the reduced polarization. The discharge capacity of the {112} faceted Co_3O_4 plate was stable over 45 cycles, while that of the {001} faceted Co_3O_4 cube was stable for just 20 cycles (Figure 7c). These tendencies may be attributed to the different adsorption properties between Li_2O_2 and the catalyst surface depending on the presence of the Co^{3+} site. Thus, we can conclude that the Co^{3+} site in the Co_3O_4 structure is the main active site reducing ORR and OER overpotential. In addition, we believe that by reducing the catalyst fraction in the porous cathode to the usual amount or mixing our materials with carbonaceous material, the round-trip efficiency could be maximized by increasing conductivity. In addition, our Li−O_2 cells need to be optimized to prevent the side reaction and depletion of electrolytes as well as the oxidation of the Li metal anode to gain more extended cycle and higher reaction stability.

CONCLUSIONS

In summary, using insight from research on the catalytic effect of cobalt oxides due to morphological surface atomic configuration and active-site charge distribution, the {100} faceted Co_3O_4 cube enclosed by only the Co^{2+} site and the Co^{3+} site exposed {112} faceted Co_3O_4 plate were successfully synthesized under hydro- and solvothermal conditions. Then, we experimentally demonstrated for the first time that the unique angular cone-shaped Li_2O_2 could be formed by controlling the surface atom configuration of the catalyst. Finally, we suggested that the Co^{3+} site dominantly affects ORR/OER properties, enabling high round-trip efficiency and enhanced cycle stability.

ASSOCIATED CONTENT

Supporting Information

The Supporting Information is available free of charge on the ACS Publications website at DOI: 10.1021/acscatal.5b01196.

Experimental methods; XRD, SEM, and electrochemical measurements; and other related information (PDF)

AUTHOR INFORMATION

Corresponding Author

*E-mail: dake1234@dongguk.edu (Y.-M.K.).

Notes

The authors declare no competing financial interest.

ACKNOWLEDGMENTS

This work was supported by the energy efficiency and resources of the Korea Institute of Energy Technology Evaluation and Planning (KETEP) grant funded by the Ministry of Knowledge Economy, Korean government (no. 20122010100140) and the National Research Foundation of Korea (NRF) grant funded by the Korea government (MSIP) (NRF-2012M1A2A2671807). K.S. acknowledges the NRF (National Research Foundation of Korea) Grant funded by the Korean Government (NRF-2013H1A2A1033981-Global PhD Fellowship Program).

REFERENCES

(1) Hoffmann, M. R.; Martin, S. T.; Choi, W.; Bahnemann, D. W. *Chem. Rev.* **1995**, *95*, 69−96.
(2) Wang, Z. L.; Song, J. *Science* **2006**, *312*, 242−246.
(3) Lu, A.-H.; Salabas, E. L.; Schüth, F. *Angew. Chem., Int. Ed.* **2007**, *46*, 1222−1244.
(4) Ando, M.; Kadono, K.; Haruta, M.; Sakaguchi, T.; Miya, M. *Nature* **1994**, *374*, 625−627.
(5) Poizot, P.; Laruelle, S.; Grugeon, S.; Dupont, L.; Tarascon, J. M. *Nature* **2000**, *407*, 496−499.
(6) Yang, P.; Zhao, D.; Margolese, D. I.; Chmelka, B. F.; Stucky, G. D. *Nature* **1998**, *396*, 152−155.
(7) Matsumoto, Y.; Murakami, M.; Shono, T.; Hasegawa, T.; Fukumura, T.; Kawasaki, M.; Ahmet, P.; Chikyow, T.; Koshihara, S.; Koinuma, H. *Science* **2001**, *291*, 854−856.
(8) Terasaki, I.; Sasago, Y.; Uchinokura, K. *Phys. Rev. B: Condens. Matter Mater. Phys.* **1997**, *56*, R12685−R12687.
(9) Vayssieres, L. *Adv. Mater.* **2003**, *15*, 464−466.
(10) Song, K.; Seo, D.-H.; Jo, M. R.; Kim, Y.-I.; Kang, K.; Kang, Y. M. *J. Phys. Chem. Lett.* **2014**, *5*, 1368−1373.
(11) Song, K.; Yoo, S.; Kang, K.; Heo, H.; Kang, Y.-M.; Jo, M.-H. *J. Power Sources* **2013**, *229*, 229−233.
(12) Comini, E. *Anal. Chim. Acta* **2006**, *568*, 28−40.
(13) Beydoun, D.; Amal, R.; Low, G. K.-C.; McEvoy, S. *J. Phys. Chem. B* **2000**, *104*, 4387−4396.
(14) Ando, M.; Kobayashi, T.; Iijima, S.; Haruta, M. *J. Mater. Chem.* **1997**, *7*, 1779−1783.
(15) Li, Y.; Tan, B.; Wu, Y. *Nano Lett.* **2008**, *8*, 265−270.
(16) Hutchins, M. G.; Wright, P. J.; Grebenik, P. D. *Sol. Energy Mater.* **1987**, *16*, 113−131.
(17) Salunkhe, R. R.; Tang, J.; Kamachi, Y.; Nakato, T.; Kim, J. H.; Yamauchi, Y. *ACS Nano* **2015**, *9*, 6288−6296.
(18) Roth, W. L. *J. Phys. Chem. Solids* **1964**, *25*, 1−10.
(19) Zakaria, M. B.; Hu, M.; Imura, M.; Salunkhe, R. R.; Umezawa, N.; Hamoudi, H.; Belik, A. A.; Yamauchi, Y. *Chem. - Eur. J.* **2014**, *20*, 17375−17384.
(20) Tan, S.; Moro-Oka, Y.; Ozaki, A. *J. Catal.* **1970**, *17*, 132−142.
(21) Xie, X.; Li, Y.; Liu, Z.-Q.; Haruta, M.; Shen, W. *Nature* **2009**, *458*, 746−749.
(22) Yan, N.; Chen, Q.; Wang, F.; Wang, Y.; Zhong, H.; Hu, L. *J. Mater. Chem. A* **2013**, *1*, 637−643.
(23) Hu, L.; Sun, K.; Peng, Q.; Xu, B.; Li, Y. *Nano Res.* **2010**, *3*, 363−368.
(24) Wang, H.; Teng, Y.; Radhakrishnan, L.; Nemoto, Y.; Imura, M.; Shimakawa, Y.; Yamauchi, Y. *J. Nanosci. Nanotechnol.* **2011**, *11*, 3843−3850.
(25) Xue, L.; Zhang, C.; He, H.; Teraoka, Y. *Appl. Catal., B* **2007**, *75*, 167−174.
(26) Ayoub, M.; Irfan, M. F.; Abdullah, A. Z. *Environ. Prog. Sustainable Energy* **2012**, *31*, 553−557.
(27) Zafeiratos, S.; Dintzer, T.; Teschner, D.; Blume, R.; Hävecker, M.; Knop-Gericke, A.; Schlögl, R. *J. Catal.* **2010**, *269*, 309−317.
(28) Hu, L.; Peng, Q.; Li, Y. *J. Am. Chem. Soc.* **2008**, *130*, 16136−16137.
(29) Jiang, S.; Song, S. *Appl. Catal., B* **2013**, *140*, 1−8.
(30) Li, Y.; Shen, W. *Chem. Soc. Rev.* **2014**, *43*, 1543−1574.
(31) Xie, X.; Shen, W. *Nanoscale* **2009**, *1*, 50−60.
(32) Xiao, J.; Kuang, Q.; Yang, S.; Xiao, F.; Wang, S.; Guo, L. *Sci. Rep.* **2013**, *3*, 2300−2307.
(33) Sun, H.; Ang, H. M.; Tadé, M. O.; Wang, S. *J. Mater. Chem. A* **2013**, *1*, 14427−14442.
(34) Li, L.; Chai, S.-H.; Dai, S.; Manthiram, A. *Energy Environ. Sci.* **2014**, *7*, 2630−2636.

DOI: 10.1021/acscatal.5b01196
ACS Catal. 2015, 5, 5116−5122

(35) Beattie, S. D.; Manolescu, D. M.; Blair, S. L. *J. Electrochem. Soc.* **2009**, *156*, A44−A47.
(36) Rioux, R. M.; Song, H.; Hoefelmeyer, J. D.; Yang, P.; Somorjai, G. A. *J. Phys. Chem. B* **2005**, *109*, 2192−2202.
(37) Zhang, B.; Wang, D.; Hou, Y.; Yang, S.; Yang, X. H.; Zhong, J. H.; Liu, J.; Wang, H. F.; Hu, P.; Zhao, H. J.; Yang, H. G. *Sci. Rep.* **2013**, *3*, 1836.
(38) Su, D.; Ford, M.; Wang, G. *Sci. Rep.* **2012**, *2*, 924.
(39) Wang, J. X.; Inada, H.; Wu, L.; Zhu, Y.; Choi, Y. M.; Liu, P.; Zhou, W.-P.; Adzic, R. R. *J. Am. Chem. Soc.* **2009**, *131*, 17298−17302.
(40) Russell, A. J.; Fersht, A. R. *Nature* **1987**, *328*, 496−500.
(41) Kauffman, D. R.; Alfonso, D.; Matranga, C.; Ohodnicki, P.; Deng, X.; Siva, R. C.; Zeng, C.; Jin, R. *Chem. Sci.* **2014**, *5*, 3151−3157.
(42) Radin, M. D.; Siegel, D. J. *Energy Environ. Sci.* **2013**, *6*, 2370−2379.
(43) Stamenkovic, V. R.; Mun, B. S.; Mayrhofer, K. J. J.; Ross, P. N.; Markovic, N. M.; Rossmeisl, J.; Greeley, J.; Nørskov, J. K. *Angew. Chem., Int. Ed.* **2006**, *45*, 2897−2901.
(44) Bruce, P. G.; Freunberger, S. A.; Hardwick, L. J.; Tarascon, J.-M. *Nat. Mater.* **2012**, *11*, 19−29.
(45) Park, M.; Sun, H.; Lee, H.; Lee, J.; Cho, J. *Adv. Energy Mater.* **2012**, *2*, 780−800.
(46) Lu, Y.-C.; Kwabi, D. G.; Yao, K. P. C.; Harding, J. R.; Zhou, J.; Zuin, L.; Shao-Horn, Y. *Energy Environ. Sci.* **2011**, *4*, 2999−3007.
(47) Zhang, S. S.; Foster, D.; Read, J. *J. Power Sources* **2010**, *195*, 1235−1240.
(48) Debart, A.; Paterson, A. J.; Bao, J.; Bruce, P. G. *Angew. Chem., Int. Ed.* **2008**, *47*, 4521−4524.
(49) Debart, A.; Bao, J.; Armstrong, G.; Bruce, P. G. *J. Power Sources* **2007**, *174*, 1177−1182.
(50) Choi, R.; Jung, J.; Kim, G.; Song, K.; Kim, Y.-I.; Jung, S. C.; Han, Y.-K.; Song, H.; Kang, Y.-M. *Energy Environ. Sci.* **2014**, *7*, 1362−1368.
(51) Song, K.; Jung, J.; Heo, Y.-U.; Lee, Y. C.; Cho, K.; Kang, Y.-M. *Phys. Chem. Chem. Phys.* **2013**, *15*, 20075−20079.
(52) Jung, J.; Song, K.; Bae, D. R.; Lee, S. W.; Lee, G.; Kang, Y.-M. *Nanoscale* **2013**, *5*, 11845−11849.
(53) Kim, B. G.; Kim, H.-J.; Back, S.; Nam, K. W.; Jung, Y.; Han, Y.-K.; Choi, J. W. *Sci. Rep.* **2014**, *4*, 4225.
(54) Debart, A.; Bao, J.; Armstrong, G.; Bruce, P. G. *J. Power Sources* **2007**, *174*, 1177−1182.
(55) Gallant, B. M.; Kwabi, D. G.; Mitchell, R. R.; Zhou, J.; Thompson, C. V.; Shao-Horn, Y. *Energy Environ. Sci.* **2013**, *6*, 2518−2528.
(56) Mitchell, R. R.; Gallant, B. M.; Shao-Horn, Y.; Thompson, C. V. *J. Phys. Chem. Lett.* **2013**, *4*, 1060−1064.
(57) Zhong, L.; Mitchell, R.; Liu, Y.; Gallant, B.; Thompson, C. V.; Huang, J. Y.; Mao, S.; Shao-Horn, Y. *Nano Lett.* **2013**, *13*, 2209−2214.
(58) Mitchell, R. R.; Gallant, B. M.; Shao-Horn, Y.; Thompson, C. V. *J. Phys. Chem. Lett.* **2013**, *4*, 1060−1064.
(59) Oh, S. H.; Black, R.; Pomerantseva, E.; Lee, J.-H.; Nazar, L. F. *Nat. Chem.* **2012**, *4*, 1004−1010.
(60) Hummelshøj, J. S.; Luntz, A. C.; Nørskov, J. K. *J. Chem. Phys.* **2013**, *138*, 034703.
(61) Liu, D.; Wang, X.; Wang, X.; Tian, W.; Bando, Y.; Golberg, D. *Sci. Rep.* **2013**, *3*, 2543−2548.
(62) Xiao, X.; Liu, X.; Zhao, H.; Chen, D.; Liu, F.; Xiang, J.; Hu, Z.; Li, Y. *Adv. Mater.* **2012**, *24*, 5762−5766.
(63) Momma, K.; Izumi, F. *J. Appl. Crystallogr.* **2008**, *41*, 653−658.

DOI: 10.1021/acscatal.5b01196
ACS Catal. 2015, 5, 5116−5122